J. Plasma Phys. (2023), *vol*. 89, 905890212 © The Author(s), 2023.
Published by Cambridge University Press
doi:10.1017/S0022377823000296

Application scope of the reductive perturbation method to derive the KdV equation and CKdV equation in dusty plasma

Heng Zhang[1],†, Yu-Xi Chen[1], Lin Wei[1], Fang-Ping Wang[1], Wei-Ping Zhang[1] and Wen-Shan Duan[1],†

[1]College of Physics and Electronic Engineering, Northwest Normal University, Lanzhou 730070, PR China

(Received 18 November 2022; revised 17 March 2023; accepted 17 March 2023)

The application scopes of two different reductive perturbation methods to derive the Korteweg–de Vries (KdV) equation and coupled KdV (CKdV) equation in two-temperature-ion dusty plasma are given by using the particle-in-cell (PIC) numerical method in the present paper. It suggests that the reductive perturbation method (RPM) is valid if the amplitude of the CKdV solitary wave is small enough. However, for the KdV solitary wave, RPM is valid not only if the amplitude of the KdV solitary wave is small enough, but also if the nonlinear coefficient of the KdV equation is not tending to zero.

Key words: dusty plasmas, plasma waves, plasma simulation

1. Introduction

Dusty plasmas usually contain highly negatively charged dust particles, electrons, ions as well as neutrals. Sometimes, there are different kinds of dust particles and different kinds of ions in a dusty plasma. Tremendous progress in dusty plasmas has been made to date (Kalman, Rosenberg & DeWitt 2000; Shukla 2001; Xie & He 2001; Wang & Wu 2002; Fortov *et al.* 2005; Shukla & Eliasson 2009; Teng *et al.* 2009; Couëdel *et al.* 2010; Ghorui, Chatterjee & Wong 2013; Ghorui *et al.* 2014; Merlino 2014; Han *et al.* 2015; Seadawy 2015). The remarkable feature of a dusty plasma is that there are low-frequency waves (Rao, Shukla & Yu 1990; Shukla 1992; Barkan, Merlino & D'Angelo 1995; Pieper & Goree 1996; Praburam & Goree 1996; Merlino *et al.* 1998; Bandyopadhyay *et al.* 2008; Dubinov & Sazonkin 2013; Kumar Tiwari & Sen 2016; Verheest & Hereman 2019).

Many researchers focused on the nonlinear solitary waves in a dusty plasma (El-Labany *et al.* 2004; Bandyopadhyay *et al.* 2008; Emamuddin, Yasmin & Mamun 2013). A solitary wave was first discovered in 1834. Later, a Korteweg–de Vries (KdV) equation was proposed in 1895 (Korteweg & De Vries 1895). However, until Kruskal and Zabusky discovered a solitary wave solution from a KdV equation in 1965 (Zabusky & Kruskal 1965; Olivier, Verheest & Maharaj 2016), different methods such as the perturbation method were used to study the nonlinear solitary waves. After that, solitary waves were found nearly in all branches of physics, especially in plasma physics (Washimi & Taniuti

† Email addresses for correspondence: zhangheng@nwnu.edu.cn, duanws@nwnu.edu.cn

1966), fluid dynamics (Ono 1991; Duan, Wang & Wei 1996), nonlinear lattice (Zabusky & Kruskal 1965; Wadati 1990), Bose–Einstein condensates (Huang, Velarde & Makarov 2001), etc.

Recently, the application scope of the perturbation method (Lee 2012; Olivier *et al.* 2016) is studied by using the one-dimensional particle-in-cell (PIC) code (Qi *et al.* 2014; Zhang *et al.* 2014, 2015; Gao *et al.* 2017; Zhang *et al.* 2017; Wang *et al.* 2018). A critical point of the reductive perturbation parameter ϵ^* is found. If the perturbation parameter $\epsilon < \epsilon^*$, the reductive perturbation method is valid, while if $\epsilon > \epsilon^*$, the reductive perturbation method is no longer reasonable (Qi *et al.* 2014; Zhang *et al.* 2014).

As is well known, many nonlinear equations can be reduced to a more simple nonlinear equation, such as the KdV equation, by using the reductive perturbation method (RPM) under small amplitude and long wavelength approximation. However, in some cases, the reductive perturbation method is invalid to derive a KdV equation. In the present paper, we will show that the reductive perturbation method is invalid when the nonlinear coefficient of the KdV tends to zero. Due to this reason, we choose another different reductive perturbation method to derive a coupled KdV (CKdV) equation. Furthermore, we find that a larger amplitude of the solitary wave results in a greater deviation between the numerical results and the theoretical results, i.e. the RPM is valid if the amplitude of the CKdV solitary wave is small enough. However, for the KdV solitary wave, the RPM is valid not only if the amplitude of the KdV solitary wave is small enough, but also if the parameters have to be limited.

2. Theoretical model

We now focus on the dust acoustic waves in two-temperature-ion dusty plasma containing highly negatively charged dust particles, electrons and two different kinds of ions (high-temperature ions and low-temperature ions). Charge neutrality at equilibrium reads $n_{il0} + n_{ih0} = Z_{d0} n_{d0} + n_{e0}$, where n_{il0}, n_{ih0}, n_{e0} and n_{d0} are the number densities of unperturbed low-temperature ion, high-temperature ion, electron and the dust particles, respectively. Here, Z_{d0} is the unperturbed number of charges residing on the dust grain measured in the units of electron charge.

For convenience and generality, we assumed that the dusty plasma is unmagnetized and collisionless. The waves propagate in the x direction. In this case, the dust fluid satisfies the following equations:

$$\frac{\partial n_d}{\partial t} + \frac{\partial (n_d u_d)}{\partial x} = 0, \tag{2.1}$$

$$\frac{\partial u_d}{\partial t} + u_d \frac{\partial u_d}{\partial x} + \frac{1}{n_d m_d} \frac{\partial p_d}{\partial x} = \frac{Z_d e}{m_d} \frac{\partial \phi}{\partial x}, \tag{2.2}$$

$$\frac{\partial^2 \phi}{\partial x^2} = \frac{e}{\epsilon_0} \left(Z_d n_d + n_e - n_{il} - n_{ih} \right), \tag{2.3}$$

where n_d, m_d, u_d and p_d refer to the number density, the mass, the velocity and the pressure of dust grain fluid, respectively. Here, Z_{d0} is the number of charge measured in units of electron charge e when a dusty plasma is in the equilibrium state. We assume $Z_d = Z_{d0}$. Additionally, ϕ is the electrostatic potential. We also assume that the electron number density (n_e), the low temperature ion number density (n_{il}) and the high temperature ion number density (n_{ih}) satisfy the Boltzmann distributions, i.e. $n_e = n_{e0} \exp(e\phi/kT_e)$, $n_{il} = n_{il0} \exp(-e\phi/kT_{il})$ and $n_{ih} = n_{ih0} \exp(-e\phi/kT_{ih})$, where T_e, T_{il}, T_{ih} and k refer to the temperatures of the electrons, the low temperature ions, the high temperature ions and the Boltzmann constant, respectively.

https://doi.org/10.1017/S0022377823000296 Published online by Cambridge University Press

Before normalization, we define an effective temperature as follows:

$$\frac{1}{T_{\text{eff}}} = \frac{1}{Z_{d0}n_{d0}}\left(\frac{n_{e0}}{T_e} + \frac{n_{il0}}{T_{il}} + \frac{n_{ih0}}{T_{ih}}\right). \tag{2.4}$$

All physical quantities are normalized as follows: the dust grain number density n_d is normalized by n_{d0}, the electron number density and ion number density are normalized by $Z_{d0}n_{d0}$, the pressure of dust grain fluid p_d is normalized by $Z_{d0}n_{d0}T_d$ and the charge of the dust grain is normalized by Z_{d0}. The space coordinates x, time t, velocity u_d and electrostatic potential ϕ are normalized by the Debye length $\lambda_D = (k\epsilon_0 T_{\text{eff}}/n_{d0}z_{d0}e^2)^{1/2}$, the inverse of dust plasma frequency $\omega^{-1} = (\epsilon_0 m_d/n_{d0}{Z_{d0}}^2e^2)^{1/2}$, the dust-acoustic speed $c_d = (kz_{d0}T_{\text{eff}}/m_d)^{1/2}$ and kT_{eff}/e, respectively. Here, T_d is the temperature of the dust grain fluid. We assumed that the equation of state of the dust grain fluid is $p_d = n_d kT_d$ and the process is approximately adiabatic, i.e. $p_d = cn_d^{\gamma}$. Then (2.1)–(2.3) become

$$\frac{\partial n_d}{\partial t} + \frac{\partial (n_d u_d)}{\partial x} = 0, \tag{2.5}$$

$$\frac{\partial u_d}{\partial t} + u_d\frac{\partial u_d}{\partial x} + \frac{\gamma'}{n_d}\frac{\partial n_d}{\partial x} = \frac{\partial \phi}{\partial x}, \tag{2.6}$$

$$\frac{\partial^2 \phi}{\partial x^2} = n_d + n_e - n_{il} - n_{ih}, \tag{2.7}$$

where $\gamma' = \gamma T_d/Z_{d0}T_{\text{eff}}$. Here, $n_e = \upsilon e^{s\beta_1\phi}$, $n_{il} = \mu_l e^{-s\phi}$ and $n_{ih} = \mu_h e^{-s\beta_2\phi}$ refer to the dimensionless number densities of electrons, lower temperature ions and higher temperature ions, respectively, with $\upsilon = n_{e0}/(Z_{d0}n_{d0})$, $\mu_l = n_{il0}/(Z_{d0}n_{d0})$, $\mu_h = n_{ih0}/(Z_{d0}n_{d0})$, $\beta_1 = T_{il}/T_e$, $\beta_2 = T_{il}/T_{ih}$ and $s = 1/(\upsilon\beta_1 + \mu_1 + \mu_h\beta_2)$.

3. Nonlinear waves

3.1. *Derivation of the KdV equation*

We now use the reductive perturbation method to study the dust acoustic solitary waves in the limited case where the wave amplitude is small but finite, while the wavelength is long enough.

We introduce new coordinates of $\xi = \epsilon(x - v_0 t)$ and $\tau = \epsilon^3 t$, where ϵ is a small parameter characterizing the order of the wavenumber and v_0 is the velocity of the dust acoustic solitary waves. The physical quantities in the system are expanded as follows: $n_d = 1 + \epsilon^2 n_{d1} + \epsilon^4 n_{d2} + \cdots$, $u_d = \epsilon^2 u_{d1} + \epsilon^4 u_{d2} + \cdots$ and $\phi = \epsilon^2\phi_1 + \epsilon^4\phi_2 + \cdots$. Substituting these expansions into normalized equations (2.5)–(2.7) and collecting the terms in different powers of ϵ, we obtain the following equations: $n_{d1} = -\phi_1$, $u_{d1} = -v_0\phi_1$, ${v_0}^2 = 1 + \gamma'$ and the KdV equation

$$\frac{\partial \phi_1}{\partial \tau} + A\phi_1\frac{\partial \phi_1}{\partial \xi} + B\frac{\partial^3 \phi_1}{\partial \xi^3} = 0, \tag{3.1}$$

where $A = -(1/2v_0)[3 + 2\gamma' + (\upsilon{\beta_1}^2 - \mu_l - \mu_h{\beta_2}^2)s^2]$ and $B = 1/2v_0$.

One of the important solutions of the KdV equation (3.1) is a single solitary wave solution as follows:

$$\phi_1 = \phi_m \text{sech}^2\frac{\xi - u_0\tau}{W}, \tag{3.2}$$

https://doi.org/10.1017/S0022377823000296 Published online by Cambridge University Press

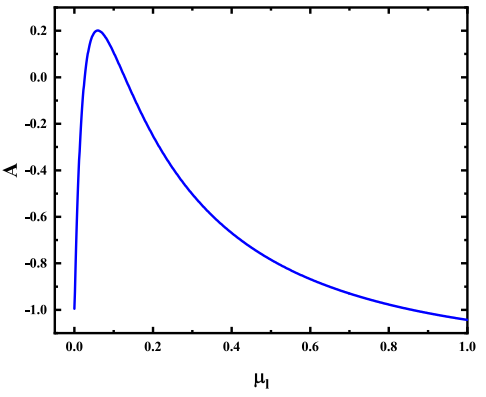

FIGURE 1. Dependence of A on μ_l, where the parameters are $T_e = 5\,\text{eV}$, $T_{il} = 0.3\,\text{eV}$, $T_{ih} = 4\,\text{eV}$, $T_d = 200\,\text{eV}$, $Z_{d0} = 1000$, $n_{d0} = 1 \times 10^{12}\,\text{m}^{-3}$ and $n_{ih0} = 1 \times 10^{15}\,\text{m}^{-3}$.

where $\phi_m = 3u_0/A$ and $W = \sqrt{4B/u_0}$. Rewriting (3.2) in experimental coordinates by $\xi = \epsilon(x - v_0 t)$ and $\tau = \epsilon^3 t$, we have

$$\phi_1 = \frac{3u_0}{A}\text{sech}^2\frac{x - \left(v_0 + u_0\epsilon^2\right)t}{\sqrt{\dfrac{4B}{u_0\epsilon^2}}}. \tag{3.3}$$

We also know that $n_{d1} = -\phi_1$, $u_{d1} = -v_0\phi_1$ and the physical quantities in the system are expanded as follows: $n_d = 1 + \epsilon^2 n_{d1} + \epsilon^4 n_{d2} + \cdots$, $u_d = \epsilon^2 u_{d1} + \epsilon^4 u_{d2} + \cdots$ and $\phi = \epsilon^2\phi_1 + \epsilon^4\phi_2 + \cdots$. Then we consider the lower order terms, and we can obtain the following equations:

$$\phi = \frac{3u_0\epsilon^2}{A}\text{sech}^2\frac{x - \left(v_0 + u_0\epsilon^2\right)t}{\sqrt{\dfrac{4B}{u_0\epsilon^2}}}, \tag{3.4}$$

$$n_d = 1 - \frac{3u_0\epsilon^2}{A}\text{sech}^2\frac{x - \left(v_0 + u_0\epsilon^2\right)t}{\sqrt{\dfrac{4B}{u_0\epsilon^2}}}, \tag{3.5}$$

$$u_d = -v_0\frac{3u_0\epsilon^2}{A}\text{sech}^2\frac{x - \left(v_0 + u_0\epsilon^2\right)t}{\sqrt{\dfrac{4B}{u_0\epsilon^2}}}, \tag{3.6}$$

where $\phi_m = 3u_0\epsilon^2/A$, $W = \sqrt{4B/u_0\epsilon^2}$ are the amplitude and the width of the KdV solitary wave, respectively.

3.2. *Derivation of the CKdV equation*

It seems that the amplitude of the solitary wave solution of the KdV equation can be infinity when $A = 0$. There is no physical meaning in this case. Therefore, the reductive perturbation is invalid in this case. Due to this reason, figure 1 shows the dependence of A on μ_l. Notice from figure 1 that A can be negative, zero and positive.

Because A can be zero, the KdV solitary wave solution may be invalid. Due to this reason, we now try to use the other method to find the nonlinear wave solution when

https://doi.org/10.1017/S0022377823000296 Published online by Cambridge University Press

$A = 0$ or A tends to zero. For this purpose, we use the following expansions (Duan & Shi 2003): $n_d = 1 + \epsilon n_{d1} + \epsilon^2 n_{d2} + \epsilon^3 n_{d3} + \cdots$, $u_d = \epsilon u_{d1} + \epsilon^2 u_{d2} + \epsilon^3 u_{d3} + \cdots$, $\phi = \epsilon\phi_1 + \epsilon^2\phi_2 + \epsilon^3\phi_3 + \cdots$. Substituting these expansions into (2.5)–(2.7) and collecting the terms in different powers of ϵ, we obtain the following equations at the different orders: $n_{d1} = -\phi_1$, $u_{d1} = -v_0\phi_1$, ${v_0}^2 = 1 + \gamma'$ and a modified KdV (MKdV) equation as

$$\frac{\partial\phi_1}{\partial\tau} + C{\phi_1}^2\frac{\partial\phi_1}{\partial\xi} + B\frac{\partial^3\phi_1}{\partial\xi^3} = 0, \tag{3.7}$$

where $B = 1/2v_0$, $C = (1/2v_0)(15 + 26\gamma' + 12\gamma'^2)$.

If A is small enough, but not zero, we use the same perturbation method as that to derive the MKdV equation (Duan & Shi 2003). We then obtain a CKdV equation as follows:

$$\frac{\partial\phi_1}{\partial\tau} + A\phi_1\frac{\partial\phi_1}{\partial\xi} + C{\phi_1}^2\frac{\partial\phi_1}{\partial\xi} + B\frac{\partial^3\phi_1}{\partial\xi^3} = 0, \tag{3.8}$$

where $A = -(1/2v_0)[3 + 2\gamma' + (v{\beta_1}^2 - \mu_l - \mu_h{\beta_2}^2)s^2]$, $B = 1/2v_0$, $C = (1/2v_0)(15 + 26\gamma' + 12\gamma'^2)$ and $B > 0$, $C > 0$.

A single solitary wave solution of the CKdV equation is

$$\phi_1 = \frac{1}{a_1 + a_2\cosh[a_3(\xi - u_o\tau)]}, \tag{3.9}$$

where $a_1 = A/6u_0$, $a_2 = \sqrt{A^2 + 6Cu_0}/6u_0$ and $a_3 = \sqrt{u_0/B}$.

Rewriting (3.9) in experimental coordinates, we have

$$\phi_1 = \frac{1}{\dfrac{A}{6u_0} + \dfrac{\sqrt{A^2 + 6Cu_0}}{6u_0}\cosh\left[\sqrt{\dfrac{u_0\epsilon^2}{B}}\left(x - \left(v_0 + u_o\epsilon^2\right)t\right)\right]}. \tag{3.10}$$

We also know that $n_{d1} = -\phi_1$, $u_{d1} = -v_0\phi_1$ and the physical quantities in the system are expanded as follows: $n_d = 1 + \epsilon n_{d1} + \epsilon^2 n_{d2} + \epsilon^3 n_{d3} + \cdots$, $u_d = \epsilon u_{d1} + \epsilon^2 u_{d2} + \epsilon^3 u_{d3} + \cdots$, $\phi = \epsilon\phi_1 + \epsilon^2\phi_2 + \epsilon^3\phi_3 + \cdots$. Then we consider the lower order terms, and we can obtain the following equations:

$$\phi = \frac{\epsilon}{\dfrac{A}{6u_0} + \dfrac{\sqrt{A^2 + 6Cu_0}}{6u_0}\cosh\left[\sqrt{\dfrac{u_0\epsilon^2}{B}}\left(x - \left(v_0 + u_o\epsilon^2\right)t\right)\right]}, \tag{3.11}$$

$$n_d = 1 - \frac{\epsilon}{\dfrac{A}{6u_0} + \dfrac{\sqrt{A^2 + 6Cu_0}}{6u_0}\cosh\left[\sqrt{\dfrac{u_0\epsilon^2}{B}}\left(x - \left(v_0 + u_o\epsilon^2\right)t\right)\right]}, \tag{3.12}$$

$$u_d = -\frac{v_0\epsilon}{\dfrac{A}{6u_0} + \dfrac{\sqrt{A^2 + 6Cu_0}}{6u_0}\cosh\left[\sqrt{\dfrac{u_0\epsilon^2}{B}}\left(x - \left(v_0 + u_o\epsilon^2\right)t\right)\right]}, \tag{3.13}$$

where $\phi_m = \epsilon/(A/6u_0 + (\sqrt{A^2 + 6Cu_0})/6u_0)$ and $W = \sqrt{B/u_0\epsilon^2}$ are the amplitude and the width of the CKdV solitary wave, respectively.

https://doi.org/10.1017/S0022377823000296 Published online by Cambridge University Press

Notice that the CKdV equation (3.8) becomes the MKdV equation (3.7) in the limited case $A = 0$. Therefore, we mainly focus on the CKdV equation and its solutions in the following sections. Then we will give the numerical results of the KdV equation and CKdV equation by using the PIC numerical method in the following sections.

4. Numerical results

In this section, we will use the PIC numerical method to find the application scopes of the perturbation methods. During simulation, the dust grains are represented by a limited ensemble of super-particles (SPs), and both electrons and ions are treated as Boltzmann distributed fluids. The weight factor of SPs is S which stands for the number of real particles. Initially, SPs are uniformly distributed in the space, its initial weight parameters S and the velocities of each SP are obtained from the initial conditions. Therefore, the equation of motion of the system is Newton's equation as follows (Qi *et al.* 2014; Zhang *et al.* 2015, 2017):

$$m_{sp}\frac{\mathrm{d}v_{sp}}{\mathrm{d}t} = q_{sp}E, \tag{4.1}$$

$$\frac{\mathrm{d}x_{sp}}{\mathrm{d}t} = v_{sp}, \tag{4.2}$$

where m_{sp}, v_{sp}, q_{sp} and x_{sp} are the mass, velocity, charge and position of the SPs, respectively. In the PIC simulation, we divided the simulation region into several grid cells. The dust particles constantly exchange information with the background grid, when the dust particles move along their trajectories. At each time step, the positions and the velocities of SPs are weighted to all the grids, then we can calculate the charge density ρ_g (or electric current density J_g). Once ρ_g is obtained, the Maxwell's equations (electromagnetic model) or Poisson–Boltzmann equation (electrostatic model) will be solved numerically to derive the value of E at each grid. In the electrostatic model, $B_g = 0$. Then the field imposed on each SP can be worked out and the electric field will drive each SP according to (4.1) and (4.2), which can be solved numerically by using the leap-frog algorithm. At last, the new positions and velocities are obtained, and the procedure will repeat until the simulation is completed (Qi *et al.* 2014; Zhang *et al.* 2015). A summary of a computational cycle of the PIC method is shown in figure 2.

4.1. *Numerical results of the KdV equation*

First we simulate the solitary wave solutions of the KdV equation. The initial conditions are given by (3.5) and (3.6) at $t = 0$ as follows:

$$n_d|_{t=0} = 1 - \frac{3u_0\epsilon^2}{A}\mathrm{sech}^2\left[\sqrt{\frac{u_0\epsilon^2}{4B}}\,(x - x_0)\right], \tag{4.3}$$

$$u_d|_{t=0} = -v_0\frac{3u_0\epsilon^2}{A}\mathrm{sech}^2\left[\sqrt{\frac{u_0\epsilon^2}{4B}}\,(x - x_0)\right]. \tag{4.4}$$

The periodic boundary conditions are chosen. The simulation parameters are as follows: the spatial step is $\Delta x = 0.2$, the time step is $\Delta t = 0.004$, the number of grid cells is $N_x = 40\,000$, the number of super particles contained in each cell is 100 and the total length of the x-axis is $L_x = \Delta x N_x$, $x_0 = L_x/4$.

Figure 3 shows the numerical results of the evolutions of the KdV solitary waves at different time t, where $A = 0.37$. Notice that the solitary wave is a compressional one

https://doi.org/10.1017/S0022377823000296 Published online by Cambridge University Press

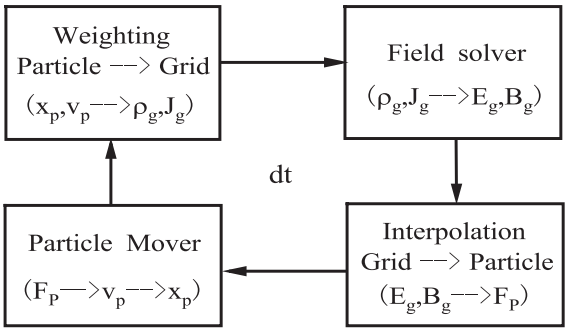

FIGURE 2. Summary of a computational cycle of the PIC method.

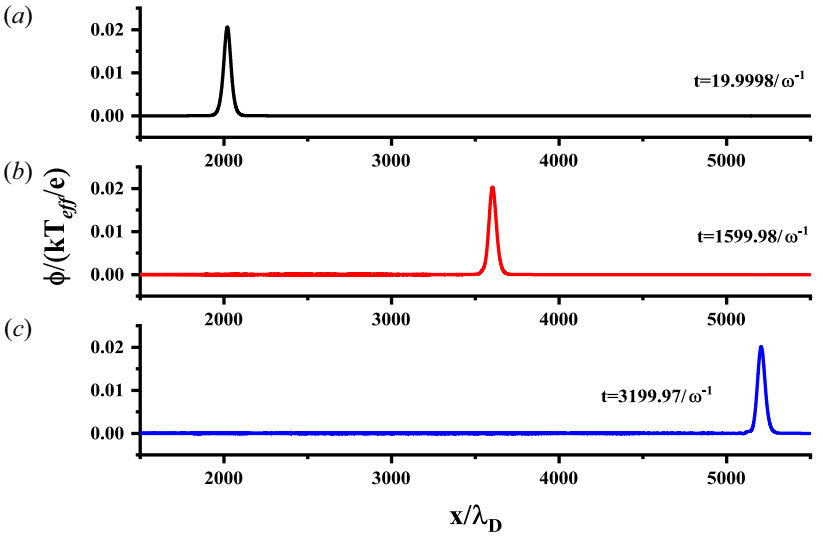

FIGURE 3. PIC simulation results of the evolution of the KdV solitary waves at different times $t = 19.9998/\omega^{-1}$, $1599.98/\omega^{-1}$, $3199.97/\omega^{-1}$, where $A = 0.37$ and the other parameters are $\epsilon = 0.05$, $\gamma = 3$, $u_0 = 1$, $x_0 = 2000$, $T_e = 5\,\text{eV}$, $T_{il} = 0.3\,\text{eV}$, $T_{ih} = 5\,\text{eV}$, $T_d = 200\,\text{eV}$, $Z_{d0} = 1000$, $n_{d0} = 1.0 \times 10^{12}\,\text{m}^{-3}$, $n_{il0} = 1.0 \times 10^{14}\,\text{m}^{-3}$ and $n_{ih0} = 1.0 \times 10^{15}\,\text{m}^{-3}$.

since $A > 0$. The comparisons between PIC simulation results and the analytical ones at different times for $A = 0.37$ are given in figure 4, which show good agreement between the two. Moreover, the numerical results are also undertaken in figure 5 for the case $A < 0$, in which the rarefactive solitary wave is obtained. Good agreements between PIC simulation results and the analytical ones are also observed in figure 6 for the rarefactive solitary wave. It indicates that our analytical results are valid. Namely, the perturbation method in this case is valid.

We now focus on the question whether the KdV solitary wave expressed by (3.1) exists when $A = 0$ or A tends to zero. Figure 7(*a–d*) shows the numerical results of the evolutions of the waves at different time t with the initial conditions of (4.3) and (4.4), where $A = 0.001$, $A = -0.001$, $A = 0.01$ and $A = -0.01$, respectively. It seems that the KdV solitary waves do not exist when A is close to zero. More numerical results suggest that the KdV solitary waves exist when $|A| > 0.06$, but do not exist if $|A| < 0.06$.

https://doi.org/10.1017/S0022377823000296 Published online by Cambridge University Press

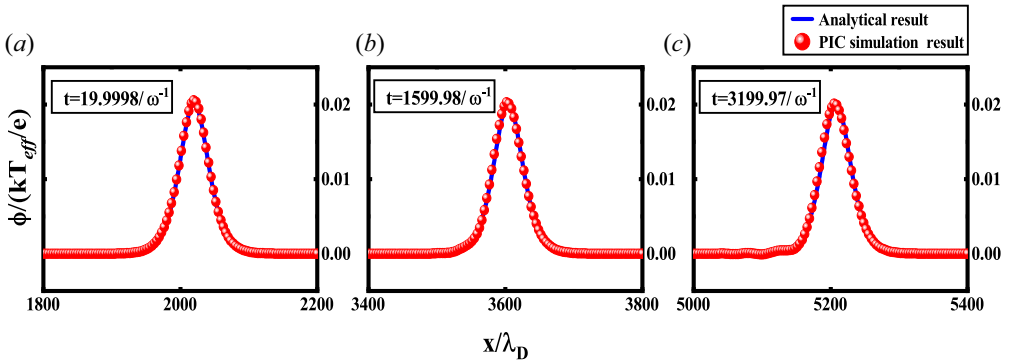

FIGURE 4. Comparisons between PIC simulation results and the analytical ones at different times $t = 19.9998/\omega^{-1}$, $1599.98/\omega^{-1}$, $3199.97/\omega^{-1}$, where $A = 0.37$ and the other parameters are $\epsilon = 0.05$, $\gamma = 3$, $u_0 = 1$, $x_0 = 2000$, $T_e = 5\,\mathrm{eV}$, $T_{il} = 0.3\,\mathrm{eV}$, $T_{ih} = 5\,\mathrm{eV}$, $T_d = 200\,\mathrm{eV}$, $Z_{d0} = 1000$, $n_{d0} = 1.0 \times 10^{12}\,\mathrm{m}^{-3}$, $n_{il0} = 1.0 \times 10^{14}\,\mathrm{m}^{-3}$ and $n_{ih0} = 1.0 \times 10^{15}\,\mathrm{m}^{-3}$.

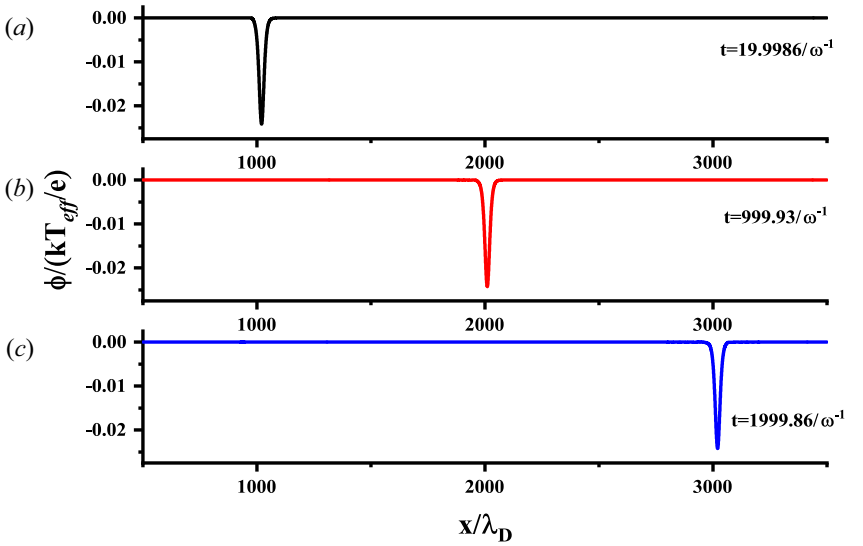

FIGURE 5. PIC simulation results of the evolution of the KdV solitary waves at different times $t = 19.9986/\omega^{-1}$, $999.93/\omega^{-1}$, $1999.86/\omega^{-1}$, where $A = -1.23$ and the other parameters are $\epsilon = 0.1$, $\gamma = 3$, $u_0 = 1$, $x_0 = 1000$, $T_e = 3\,\mathrm{eV}$, $T_{il} = 0.5\,\mathrm{eV}$, $T_{ih} = 3\,\mathrm{eV}$, $T_d = 200\,\mathrm{eV}$, $Z_{d0} = 1000$, $n_{d0} = 1.0 \times 10^{12}\,\mathrm{m}^{-3}$, $n_{il0} = 1.0 \times 10^{15}\,\mathrm{m}^{-3}$ and $n_{ih0} = 1.1 \times 10^{15}\,\mathrm{m}^{-3}$.

4.2. *Numerical results of CKdV equation*

If $A = 0$ or A tends to zero, the solution of the KdV equation is no longer valid, so we use the solution of the CKdV equation. Now we consider whether the CKdV solitary wave propagates when $A = 0$ or A tends to zero. The initial conditions are given by (3.12) and (3.13) at $t = 0$ as follows:

$$n_d|_{t=0} = 1 - \frac{\epsilon}{\dfrac{A}{6u_0} + \dfrac{\sqrt{A^2 + 6Cu_0}}{6u_0} \cosh\left[\sqrt{\dfrac{u_0\epsilon^2}{B}}\,(x - x_0)\right]}, \tag{4.5}$$

https://doi.org/10.1017/S0022377823000296 Published online by Cambridge University Press

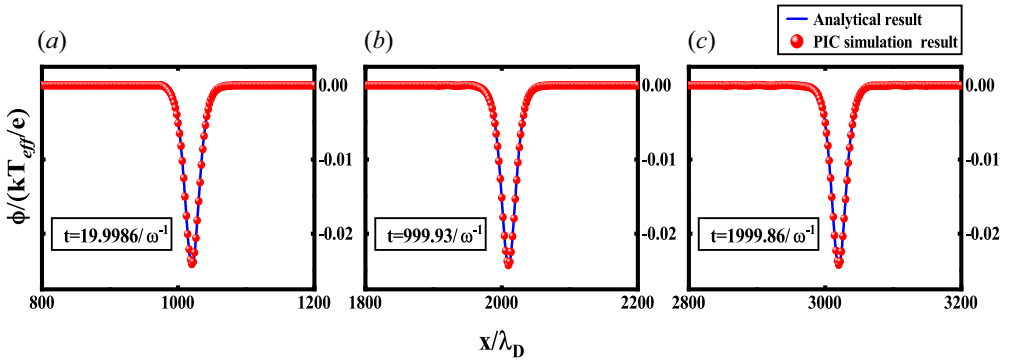

FIGURE 6. Comparisons between PIC simulation results and the analytical ones at different times $t = 19.9986/\omega^{-1}$, $999.93/\omega^{-1}$, $1999.86/\omega^{-1}$, where $A = -1.23$ and the other parameters are $\epsilon = 0.1$, $\gamma = 3$, $u_0 = 1$, $x_0 = 1000$, $T_e = 3\,\mathrm{eV}$, $T_{il} = 0.5\,\mathrm{eV}$, $T_{ih} = 3\,\mathrm{eV}$, $T_d = 200\,\mathrm{eV}$, $Z_{d0} = 1000$, $n_{d0} = 1.0 \times 10^{12}\,\mathrm{m}^{-3}$, $n_{il0} = 1.0 \times 10^{15}\,\mathrm{m}^{-3}$ and $n_{ih0} = 1.1 \times 10^{15}\,\mathrm{m}^{-3}$.

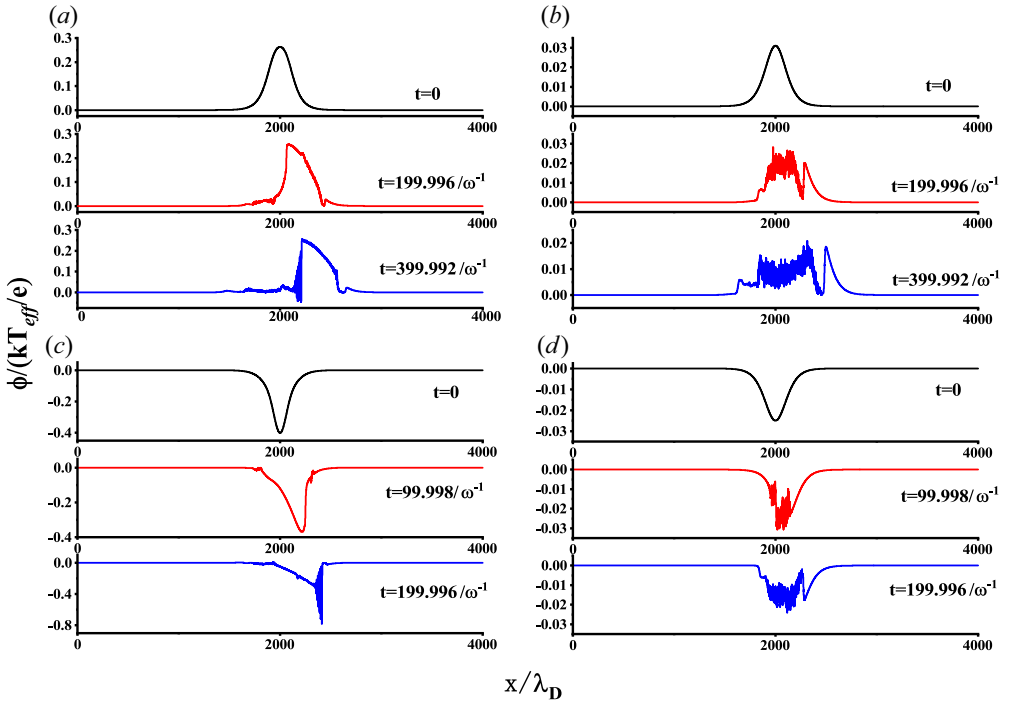

FIGURE 7. PIC simulation results of the evolution of the nonlinear waves at different times, where (*a*) $A = 0.001$; (*b*) $A = 0.01$; (*c*) $A = -0.001$; (*d*) $A = -0.01$. The other parameters are $\epsilon = 0.01$, $\gamma = 3$, $u_0 = 1$, $x_0 = 2000$, $T_e = 5\,\mathrm{eV}$, $T_{il} = 0.3\,\mathrm{eV}$, $T_{ih} = 4\,\mathrm{eV}$, $T_d = 200\,\mathrm{eV}$, $Z_{d0} = 1000$, $n_{d0} = 1.0 \times 10^{12}\,\mathrm{m}^{-3}$, $n_{ih0} = 1.0 \times 10^{15}\,\mathrm{m}^{-3}$, and $n_{il0} = 1.277 \times 10^{14}\,\mathrm{m}^{-3}$, $1.254 \times 10^{14}\,\mathrm{m}^{-3}$, $1.283 \times 10^{14}\,\mathrm{m}^{-3}$ and $1.31 \times 10^{14}\,\mathrm{m}^{-3}$ in panels (*a*,*b*,*c*,*d*), respectively.

$$u_d|_{t=0} = -\frac{v_0\epsilon}{\dfrac{A}{6u_0} + \dfrac{\sqrt{A^2 + 6Cu_0}}{6u_0}\cosh\left[\sqrt{\dfrac{u_0\epsilon^2}{B}}\,(x - x_0)\right]}. \tag{4.6}$$

https://doi.org/10.1017/S0022377823000296 Published online by Cambridge University Press

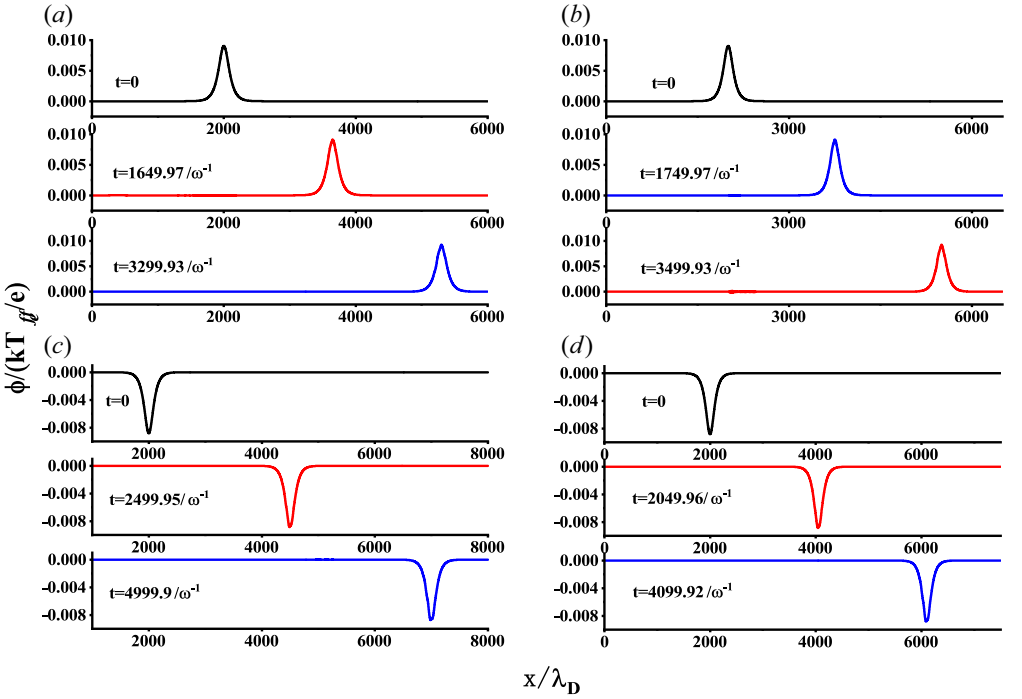

FIGURE 8. PIC simulation results of the evolution of the CKdV solitary waves at different times, where (*a*) $A = 0.001$; (*b*) $A = 0.01$; (*c*) $A = -0.001$; (*d*) $A = -0.01$. The other parameters are $\epsilon = 0.01$, $\gamma = 3$, $u_0 = 1$, $x_0 = 2000$, $T_e = 5\,\text{eV}$, $T_{il} = 0.3\,\text{eV}$, $T_{ih} = 4\,\text{eV}$, $T_d = 200\,\text{eV}$, $Z_{d0} = 1000$, $n_{d0} = 1.0 \times 10^{12}\,\text{m}^{-3}$, $n_{ih0} = 1.0 \times 10^{15}\,\text{m}^{-3}$, and $n_{il0} = 1.277 \times 10^{14}\,\text{m}^{-3}$, $1.254 \times 10^{14}\,\text{m}^{-3}$, $1.283 \times 10^{14}\,\text{m}^{-3}$ and $1.31 \times 10^{14}\,\text{m}^{-3}$ in panels (*a*,*b*,*c*,*d*), respectively.

The periodic boundary conditions are chosen. The simulation parameters are as follows: the spatial step is $\Delta x = 0.5$, the time step is $\Delta t = 0.01$, the number of grid cells is $N_x = 20000$, the number of super particles contained in each cell is 100, the total length of the x-axis is $L_x = \Delta x N_x$, $\gamma = 3$, $x_0 = L_x/5$, $u_0 = 1$ and $\epsilon = 0.01$.

Figure 8(*a–d*) shows the numerical results of the evolutions of the CKdV solitary waves at different time t, where $A = 0.001$, $A = -0.001$, $A = 0.01$ and $A = -0.01$, respectively. It shows that the CKdV solitary wave can propagate stably when $A = 0$ or A tends to zero.

4.3. *The application scope of the CKdV equation*

To further understand the CKdV solitary wave propagation for different amplitudes, we change the value of ϵ, and keep the other parameters constant (Lin & Duan 2005): $\gamma = 3$, $u_0 = 1$, $x_0 = 5000$, $T_e = 5\,\text{eV}$, $T_{il} = 0.3\,\text{eV}$, $T_{ih} = 4\,\text{eV}$, $T_d = 200\,\text{eV}$, $Z_{d0} = 1000$, $n_{d0} = 1.0 \times 10^{12}\,\text{m}^{-3}$, $n_{il0} = 1.28 \times 10^{14}\,\text{m}^{-3}$ and $n_{ih0} = 1.0 \times 10^{15}\,\text{m}^{-3}$. We will see how CKdV solitary waves vary concerning the values of the parameter ϵ.

Figure 9(*a*) shows the numerical results of the evolutions of the CKdV solitary waves at different time t when $\epsilon = 0.01$, i.e. the wave amplitude is $\phi_m = 0.009$. Figure 9(*b*) shows the comparisons between PIC simulation results and the analytical ones at different times.

Notice that the amplitude of the solitary wave remains unchanged during its propagation. Good agreements between PIC simulation results and the analytical ones are observed in figure 9(*b*).

https://doi.org/10.1017/S0022377823000296 Published online by Cambridge University Press

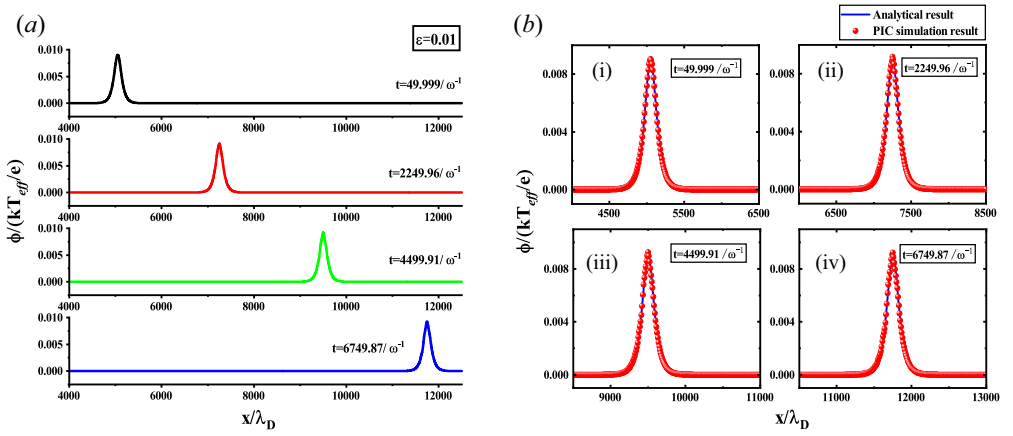

FIGURE 9. (*a*) PIC simulation results of the evolution of the CKdV solitary waves at different times, when $\epsilon = 0.01$; (*b*) comparisons between PIC simulation results and the analytical ones at different times, when $\epsilon = 0.01$.

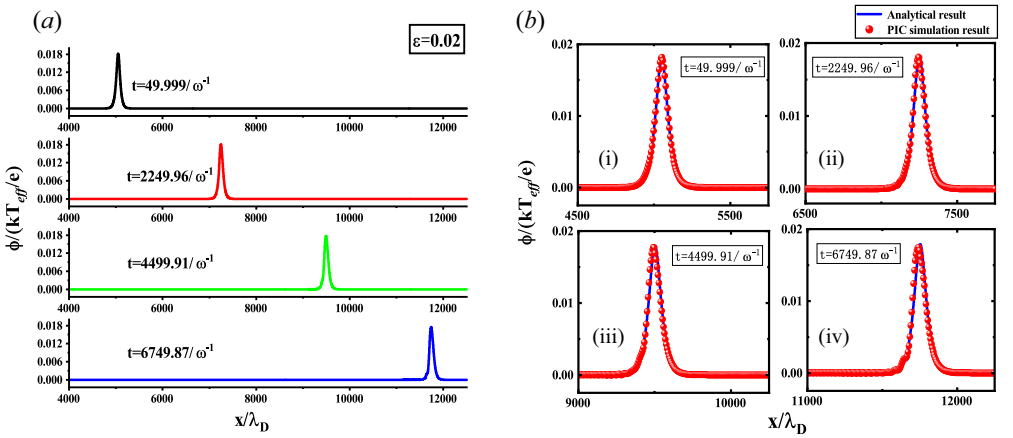

FIGURE 10. (*a*) PIC simulation results of the evolution of the CKdV solitary waves at different times, when $\epsilon = 0.02$; (*b*) comparisons between PIC simulation results and the analytical ones at different times, when $\epsilon = 0.02$.

For further study, figures 10(*a*) and 11(*a*) show the numerical results of the evolutions of the CKdV solitary waves at different times when $\epsilon = 0.02$ ($\phi_m = 0.018$) and $\epsilon = 0.03$ ($\phi_m = 0.027$), respectively. The corresponding comparisons between numerical results and the analytical ones are shown in figures 10(*b*) and 11(*b*). Good agreement between PIC numerical results and the analytical ones is observed in figures 9(*b*) and 10(*b*). However, in figure 11(*b*), differences between PIC numerical results and the analytical ones are observed.

Though the solitary wave exists, it seems from figure 11 that there are some spatial asymmetry especially for large perturbation amplitude and long-time simulation. This is due to the following reason. The expression of the solitary wave from the RPM is only valid for the small-amplitude and long-wavelength limitation. In the simulation, we use the initial condition from the expression of the solitary wave from the RPM. If the limit condition is not satisfied, for example, a large amplitude solitary wave, the real solitary

https://doi.org/10.1017/S0022377823000296 Published online by Cambridge University Press

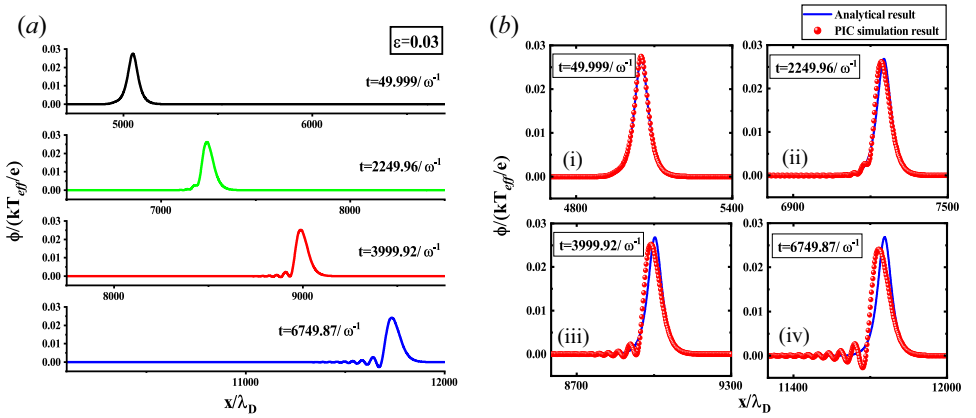

FIGURE 11. (*a*) PIC simulation results of the evolution of the CKdV solitary waves at different times, when $\epsilon = 0.03$; (*b*) comparisons between PIC simulation results and the analytical ones at different times, when $\epsilon = 0.03$.

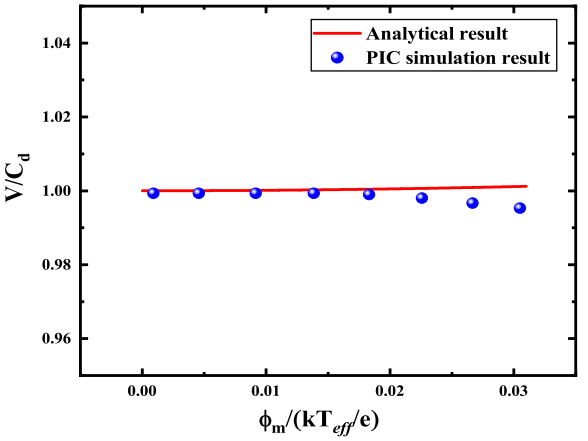

FIGURE 12. Numerical results and the analytical ones of the dependence of the propagation velocity (V/C_d) of the CKdV solitary wave on the wave amplitude ($\phi_m/(kT_{\mathrm{eff}}/e)$).

waveform is different from that of the expression of the solitary wave from the RPM. Therefore, as the solitary wave propagates, the uncorrected initial form of the solitary wave will evolve into a real solitary wave and some linear waves or radiations. Finally, spatial asymmetry in the solitary wave propagation in PIC simulations appears for large perturbation and long-time simulation.

To further understand how the differences between PIC numerical results and the analytical ones depend on the parameter ϵ, or the wave amplitude, the variations of both the numerical results and the analytical ones of the propagation velocity of solitary waves with respect to different amplitudes of solitary waves are given in figure 12.

It is noted that when the amplitude of the solitary wave is small, i.e. the parameter ϵ is small, the PIC numerical results are in good agreement with the analytical ones. However, the differences between the two are observed when the wave amplitude is large enough. Moreover, the difference between the two increases as the wave amplitude increases.

https://doi.org/10.1017/S0022377823000296 Published online by Cambridge University Press

5. Discussion and conclusion

In the present paper, two different reductive perturbation methods are used to derive the KdV equation and the CKdV equation, respectively, in two-temperature-ion dusty plasma. It is found by using the PIC numerical method that the reductive perturbation method to derive the KdV equation is invalid when the nonlinear coefficient A of the KdV equation tends to zero. The application scope of the perturbation method to derive the KdV equation with respect to the nonlinear coefficient A is given. It is noted that the KdV solitary wave does not exist when $A < 0.06$, while it exists when $A > 0.06$. However, from the numerical results, it is found that under the same parameters of the plasma, the CKdV solitary wave exists in the system even when the coefficient A is close to zero. Furthermore, we find that a larger amplitude of the solitary wave results in a greater deviation between the numerical results and the theoretical results, i.e. when the amplitude of the solitary wave is small enough, the perturbation method to derive the CKdV equation is valid. However, for the KdV solitary wave, the reductive perturbation method is only valid not only if the amplitude of the KdV solitary wave is small enough, but also if $A > 0.06$.

Acknowledgements

Editor E. Thomas Jr. thanks the referees for their advice in evaluating this article.

Funding

This work was supported by the National Natural Science Foundation of China (Nos. 11965019, 42004131) and the Foundation of Gansu Educational Committee (No. 2022QB-178).

Declaration of interests

The authors report no conflict of interest.

REFERENCES

Bandyopadhyay, P., Prasad, G., Sen, A. & Kaw, P.K. 2008 Experimental study of nonlinear dust acoustic solitary waves in a dusty plasma. *Phys. Rev. Lett*. **101** (6), 065006.

Barkan, A., Merlino, R.L. & D'Angelo, N. 1995 Laboratory observation of the dust-acoustic wave mode. *Phys. Plasmas* **2** (10), 3563–3565.

Couëdel, L., Nosenko, V., Ivlev, A.V., Zhdanov, S.K., Thomas, H.M. & Morfill, G.E. 2010 Direct observation of mode-coupling instability in two-dimensional plasma crystals. *Phys. Rev. Lett*. **104** (19), 195001.

Duan, W.S. & Shi, Y.R. 2003 The effect of dust size distribution for two ion temperature dusty plasmas. *Chaos, Solitons Fractals* **18** (2), 321–328.

Duan, W.S., Wang, B.R. & Wei, R.J. 1996 The decay of soliton in small blood artery. *J. Phys. Soc. Japan* **65** (4), 945–947.

Dubinov, A.E. & Sazonkin, M.A. 2013 Supernonlinear ion-acoustic waves in a dusty plasma. *Phys. Wave Phenomena* **21** (2), 118–128.

El-Labany, S.K., El-Taibany, W.F., Mamun, A.A. & Moslem, W.M. 2004 Dust acoustic solitary waves and double layers in a dusty plasma with two-temperature trapped ions. *Phys. Plasmas* **11** (3), 926–933.

Emamuddin, M., Yasmin, S. & Mamun, A.A. 2013 Higher order nonlinear equations for the dust-acoustic waves in a dusty plasma with two temperature-ions and nonextensive electrons. *Phys. Plasmas* **20** (4), 043705.

Fortov, V.E., Ivlev, A.V., Khrapak, S.A., Khrapak, A.G. & Morfill, G.E. 2005 Complex (dusty) plasmas: Current status, open issues, perspectives. *Phys. Rep*. **421** (1–2), 1–103.

Gao, D.N., Zhang, H., Zhang, J., Li, Z.Z. & Duan, W.S. 2017 Effect of a damping force on dust acoustic waves simulated by particle-in-cell method. *Phys. Plasmas* **24** (4), 043703.

GHORUI, M.K., CHATTERJEE, P. & WONG, C.S. 2013 Head on collision of dust ion acoustic solitary waves in magnetized quantum dusty plasmas. *Astrophys. Space Sci*. **343** (2), 639–645.

GHORUI, M.K., SAMANTA, U.K., MAJI, T.K. & CHATTERJEE, P. 2014 Head-on collisions of two types of dust-acoustic solitons in a magnetized quantum plasma. *Astrophys. Space Sci*. **352** (1), 159–169.

HAN, J.F., GAO, D.N., ZHANG, H., WANG, X.Y. & DUAN, W.S. 2015 Effects of the dust size distribution in one-dimensional quantum dusty plasma. *Front. Phys*. **10** (5), 105201.

HUANG, G.X., VELARDE, M.G. & MAKAROV, V.A. 2001 Dark solitons and their head-on collisions in Bose–Einstein condensates. *Phys. Rev.* A **64** (1), 013617.

KALMAN, G., ROSENBERG, M. & DEWITT, H.E. 2000 Collective modes in strongly correlated Yukawa liquids: waves in dusty plasmas. *Phys. Rev. Lett*. **84** (26), 6030.

KORTEWEG, D.J. & DE VRIES, G. 1895 On the change of form of long waves advancing in a rectangular canal, and on a new type of long stationary waves. *Lond. Edinb. Dublin Philos. Mag. J. Sci*. **39** (240), 422–443.

KUMAR TIWARI, S. & SEN, A. 2016 Wakes and precursor soliton excitations by a moving charged object in a plasma. *Phys. Plasmas* **23** (2), 022301.

LEE, N.C. 2012 Derivation of nonlinear Schrödinger equation for electrostatic and electromagnetic waves in fully relativistic two-fluid plasmas by the reductive perturbation method. *Phys. Plasmas* **19** (8), 082303.

LIN, M.M. & DUAN, W.S. 2005 The Kadomtsev–Petviashvili (KP), MKP, and coupled KP equations for two-ion-temperature dusty plasmas. *Chaos, Solitons Fractals* **23** (3), 929–937.

MERLINO, R.L. 2014 25 years of dust acoustic waves. *J. Plasma Phys*. **80** (6), 773–786.

MERLINO, R.L., BARKAN, A., THOMPSON, C. & D'ANGELO, N. 1998 Laboratory studies of waves and instabilities in dusty plasmas. *Phys. Plasmas* **5** (5), 1607–1614.

OLIVIER, C.P., VERHEEST, F. & MAHARAJ, S.K. 2016 A small-amplitude study of solitons near critical plasma compositions. *J. Plasma Phys*. **82** (6), 905820605.

ONO, H. 1991 Deformation of nonlinear gravity waves due to depth variation. *J. Phys. Soc. Japan* **60** (12), 4127–4132.

PIEPER, J.B. & GOREE, J. 1996 Dispersion of plasma dust acoustic waves in the strong-coupling regime. *Phys. Rev. Lett*. **77** (15), 3137.

PRABURAM, G. & GOREE, J. 1996 Experimental observation of very low-frequency macroscopic modes in a dusty plasma. *Phys. Plasmas* **3** (4), 1212–1219.

QI, X., XU, Y.X., DUAN, W.S. & YANG, L. 2014 The application scope of the reductive perturbation method and the upper limit of the dust acoustic solitary waves in a dusty plasma. *Phys. Plasmas* **21** (1), 013702.

RAO, N.N., SHUKLA, P.K. & YU, M.Y. 1990 Dust-acoustic waves in dusty plasmas. *Planet. Space Sci*. **38** (4), 543–546.

SEADAWY, A.R. 2015 Nonlinear wave solutions of the three-dimensional Zakharov–Kuznetsov–Burgers equation in dusty plasma. *Physica* A **439**, 124–131.

SHUKLA, P.K. 1992 Low-frequency modes in dusty plasmas. *Phys. Scr*. **45** (5), 504–507.

SHUKLA, P.K. 2001 A survey of dusty plasma physics. *Phys. Plasmas* **8** (5), 1791–1803.

SHUKLA, P.K. & ELIASSON, B. 2009 Colloquium: fundamentals of dust-plasma interactions. *Rev. Mod. Phys*. **81** (1), 25.

TENG, L.W., CHANG, M.C., TSENG, Y.P. & LIN, I. 2009 Wave-particle dynamics of wave breaking in the self-excited dust acoustic wave. *Phys. Rev. Lett*. **103** (24), 245005.

VERHEEST, F. & HEREMAN, W.A. 2019 Collisions of acoustic solitons and their electric fields in plasmas at critical compositions. *J. Plasma Phys*. **85** (1), 905850106.

WADATI, M. 1990 Deformation of solitons in random media. *J. Phys. Soc. Japan* **59** (12), 4201–4203.

WANG, D.Z. & WU, H.T. 2002 Analysis of dusty plasma in the positive column of glow discharges. *Chin. Phys*. **11** (8), 0799.

WANG, F.P., HAN, J.F., ZHANG, J., GAO, D.N., LI, Z.Z., DUAN, W.S. & ZHANG, H. 2018 Numerical simulation of dark envelope soliton in plasma. *Phys. Plasmas* **25** (3), 032121.

WASHIMI, H. & TANIUTI, T. 1966 Propagation of ion-acoustic solitary waves of small amplitude. *Phys. Rev. Lett*. **17** (19), 996.

XIE, B.S. & HE, K.F. 2001 Nonlinear localized structure in dusty plasma. *Chin. Phys*. **10** (3), 0214.

ZABUSKY, N.J. & KRUSKAL, M.D. 1965 Interaction of solitons in a collisionless plasma and the recurrence of initial states. *Phys. Rev. Lett*. **15** (6), 240.

ZHANG, H., QI, X., DUAN, W.S. & YANG, L. 2015 Envelope solitary waves exist and collide head-on without phase shift in a dusty plasma. *Sci. Rep*. **5** (1), 14239.

ZHANG, H., YANG, Y., HONG, X.R., QI, X., DUAN, W.S. & YANG, L. 2017 Freak oscillation in a dusty plasma. *Phys. Rev.* E **95** (5), 053207.

ZHANG, J., YANG, Y., XU, Y.X., YANG, L., QI, X. & DUAN, W.S. 2014 The study of the Poincare–Lighthill–Kuo method by using the particle-in-cell simulation method in a dusty plasma. *Phys. Plasmas* **21** (10), 103706.